Semnan University

Progress in Physics of Applied Materials

journal homepage: https://ppam.semnan.ac.ir/

Numerical Study of the Role of Nanoparticles in Breast Tumor Treatment in 3D

Abdol Jabbar Shokri [a*], Hamed Heidari [b]

[a] *Department of Science, Payame Noor University, Tehran, Iran*

[b] *Department of Physics, Varamin Region, Directorate of Education of Tehran Province, Iran*

ARTICLE INFO

Article history:
Received: 7 September 2024
Revised: 4 October 2024
Accepted: 11 October 2024

Keywords:
Magnetic Hyperthermia;
Magnetic Nanoparticles;
Breast Cancer;
Simulation;
Comsol Multiphysics.

ABSTRACT

In this paper, we conducted a numerical study to investigate the role of magnetic nanoparticles (MNPs) in the treatment of cancerous tissues in three dimensional. First, we considered the governing equations associated with this method. Next, we utilized the finite element method (FEM) and Comsol Multiphysics software package to calculate parameters such as temperature distribution, generated heat, and the fraction of damage in tumor and normal tissues over a 40-minute period. The applied frequencies and current in the coil were 150 and 300 kHz and 550 A, respectively. Our calculations revealed that the maximum temperatures of the tumor at frequencies of 150 and 300 kHz were 45.4 and 47 degrees centigrade, respectively. These temperatures are sufficient to destroy cancer cells. Furthermore, the comparison of results at 150 and 300 kHz frequencies demonstrated that parameters such as temperature, heat, and degradation rate increase with the increase of frequency. Additionally, we found that the tumor damage at the end of the process for frequencies of 150 and 300 kHz was 100% in the center of the tumor, but reduced to 63% and 75% at the border, respectively.

1. Introduction

Magnetic hyperthermia is a promising method for treating malignant tumors. Unlike lasers, ionizing rays, and microwaves, this innovative technique provides a new approach to hyperthermia. It skillfully avoids the drawbacks of traditional methods and paves the way for a novel course in medical treatment. In magnetic hyperthermia, an external magnetic field heats magnetic nanoparticles in a tumor, causing them to convert magnetic energy into thermal energy. The nanoparticles transfer heat to their surroundings, raising local temperatures to 42 to 46 degrees Celsius. This elevated temperature is able to destroy malignant cells without harming normal tissues. For hyperthermia, nanoparticles should be 10 to 100 nm in size, which allows them to penetrate biological barriers and reach damaged tissues. Modifying the size, shape, and surface of the nanoparticles can enhance their therapeutic effects [1-3].

Magnetic hyperthermia uses a method called induction heating, which is a versatile technology widely used in various industries and in medicine. It is valued for its speed, accuracy, controllability, and efficiency, which surpass other methods. A typical system includes a power supply, a frequency converter, an inductor, a control system, and a cooling system [4].

In general, heat loss in magnetic materials under an alternating magnetic field is due to: (a) eddy current loss, (b) hysteresis loss, and (c) relaxation loss (Neel and Brownian relaxation loss). Eddy currents in conductive bodies are significant. But they do not contribute to heat generation in magnetic nanoparticles. They generate very little heat in magnetic nanoparticles. Hysteresis loss heats larger ferromagnetic particles. But it is absent in single-

*** Corresponding author.**
E-mail address: *ajshokri1975@pnu.ac.ir*

Cite this article as:
Shokri, A. J., Heidari H, 2024. Numerical Study of the Role of Nanoparticles in Breast Tumor Treatment in 3D. *Progress in Physics of Applied Materials*, *5*(1), pp. 23-30. DOI: 10.22075/ppam.2024.34628.1107

domain magnetite NPs. The magnetic field should oscillate at 100-300 kHz. This low radio frequency is needed to heat cancer cells to a therapeutic temperature for destruction [5, 6].

During treatment, ensuring body safety and preventing side effects are crucial. It is important to manage body temperature and avoid overheating. Additionally, accurately predicting the magnetic field's reach is essential for the success of magnetic hyperthermia. The success of this treatment depends on several factors, including the properties of the nanoparticles, their distribution in the tumor, temperature, and the duration of heat exposure. Each type of cancer and tumor region has its specific conditions, so it is necessary to optimize and adjust these factors accordingly. This optimization is key to achieving effective treatment with minimal side effects [7, 8].

Research is currently centered on single-domain superparamagnetic (SPM) nanoparticles, which allow for improved control of heat within tumors. According to Langevin's theory, SPM nanoparticles exhibit high magnetization in a magnetic field, but lose this magnetization once the field is removed [9-11].

Recent research on hyperthermia for cancer has shown promising results. Raising the temperature in tumor areas can kill cancer cells, while sparing normal tissues [12]. Salmon et al. demonstrated that hyperthermia raises tumor temperature. This effect depends on magnetic materials, the frequency and strength of magnetic fields, blood flow, and exposure time [13]. Jorden et al. were the first to show clinical results using magnetic hyperthermia for brain tumors. They used superparamagnetic iron oxide nanoparticles coated with aminosilane. First, the magnetic fluid is injected into the tumor. Then, it is exposed to an alternating magnetic field. The heat from the nanoparticles either kills tumor cells or makes them more sensitive to radiotherapy or chemotherapy [14]. Dughiero and Corazza utilized the finite element method and Fluent software to analyze heat distribution in tumor tissue. Their findings indicated that blood flow in vessels has an impact on the heat distribution in tumors [15]. Zhao et al. employed 15 nm magnetic iron oxide nanoparticles to conduct hyperthermia treatment for head and neck cancer in mice. They investigated the temperature increase in tumor tissue through simulations and laboratory experiments. Both approaches demonstrated similar temperature elevations in the center of the tumor [16]. Byrd et al. examined the shapes of breast cancer using MRI data. They applied geometric formulas to create 3D tumor models and categorized 83 cases. The cancers were classified into four shapes: spherical, discoidal, segmental, and irregular. Only 19% of the cases were spherical, while discoidal tumors were the most prevalent, accounting for 34% [17].

In this article, the finite element method was used to solve Pennes' bio-heat transfer equation using Comsol software to predict the temperature distribution pattern in tissues. Additionally, a three-dimensional thermal bioheat transfer model based on the Arrhenius model was employed to evaluate the extent of thermal damage in tumors.

2. Materials and Methods

2.1. Governing equations

Maxwell's equations play a crucial role in the study of magnetic nanoparticles for hyperthermia. These equations provide a comprehensive framework for describing and predicting the behavior of the magnetic field and its interaction with nanoparticles. The concise representation of Maxwell's equations is given by the following relationship [12, 18]:

$$\nabla^2 A + \omega^2 \mu \varepsilon A - i\mu\omega\sigma A = -\mu J_{ext} \tag{1}$$

where, A is vector magnetic potential (Web/m), μ is magnetic permeability (H/m) ω is angular frequency (rad/s), ε is permittivity (F/m), σ is electrical conductivity (S/m), $\boldsymbol{J}_{ext}$ is applied current to the coil, and $i\left(=\sqrt{-1}\right)$ is complex unit.

Pennes' biological heat transfer equation can be used to describe the heat transfer produced by nanoparticles. In the present work, this equation is used to model heat transfer in breast tissue. The equation is as follows [19]:

$$(\rho c)_t \frac{\partial T_t}{\partial t} = \nabla \cdot (k_t \nabla T_t) + Q_{perf} + Q_{met} + Q_{ext} \tag{2}$$

where ρ, c and k are the density, specific heat and thermal conductivity of the tissue, respectively, T is temperature, t is time, and $(\nabla \cdot (k\nabla T))$ is the heat transfer term represents the heat diffusion through the tissue. It considers the tissues thermal conductivity. It measures how well heat moves within the tissue. Q_{perf} , It refers to the heat from blood perfusion. It is due to the heat transfer from blood flow in the tissue. This term considers the blood perfusion rate and the difference in temperature between the blood and the tissue. Q_{met} Metabolic heat source (450 for healthy tissue, 29000 for tumor tissue), and Q_{ext} external heat source is the heat from the magnetic nanoparticles. The heat produced in the tumor tissue by magnetic nanoparticles is given by the following relationship [20]:

$$p = \mu_0 \pi \chi_0 f H_0^2 \frac{2\pi f\tau}{1+(2\pi f\tau)^2} \tag{3}$$

where μ_0 is the permeability of free space, χ_0 is the magnetic susceptibility, H_0 is the amplitude, f is the frequency of the alternating magnetic field, and τ its effective time are given by the following relationship [21, 22]:

$$\tau^{-1} = \tau_N^{-1} + \tau_B^{-1} \tag{4}$$

where τ_N and τ_B are the relaxation times of Neel and Brownian, respectively, and have values of 2.15×10^{-6} and 2×10^{-2} respectively.

Relaxation times of Neel, which is actually the relationship between thermal energy and anisotropy, is given by the following relationship: [23].

$$\tau_N = \frac{\tau_0}{2}\sqrt{\pi\frac{k_BT}{KV}}exp(\frac{KV}{k_BT}) \quad (5)$$

where $k_B$is Boltzmann's constant, T is temperature, K is anisotropy constant, V is volume of nanoparticles, and $\frac{KV}{k_BT}$ is the ratio of heat energy to anisotropy energy.

Brownian motion is related to the rotation of nanoparticles in the medium in which they are placed and is given by the following equation:

$$\tau_B = \frac{3\eta V_H}{k_BT} \quad (6)$$

where V_H is the hydrodynamic volume of magnetic nanoparticles and η is the viscosity of the environment.

Hence, it can be inferred that Brownian motion is primarily influenced by the viscosity of the medium. Furthermore, the extent of tumor tissue destruction has been quantified using the destruction integral and the first-order Arrhenius equation. This equation describes the relationship between tissue mortality, temperature, and treatment duration as follows [15, 16]:

$$\Omega(t) = \int_0^t A e^{\frac{E_a}{RT}} dt \quad (7)$$

where T is the temperature calculated inside the calculation domain due to heat RF, $t(s)$ is the erosion time, $A(s^{-1})$ is the frequency factor (1.18×10^{44}), $E_a(J/mol)$ is the activation energy for destruction reaction (3.02×10^5) irreversible and R is the global gas constant (8.3145). it is other parameters are shown in Table 1.

Table 1. Values of parameters used [24]

Parameter	$\rho\ [\frac{kg}{m^3}]$	$c\ [\frac{J}{kg.K}]$	$k\ [\frac{W}{m.K}]$
Normal	1080	3500	0.5107
Tumor	1060	3000	0.4503
Blood	1050	4180	0.51
Fe_3O_4	5180	4000	40

2.2. Conditions calculations

In order to describe the problem conditions, we are assuming the presence of a spherical tumor with a radius of 10 mm. This tumor is located approximately 10 mm beneath the layers of the dermis, epidermis, hypodermis, and adjacent tissue in the skin. Fig. 1 depicts the meshing and tumor geometry within the three-dimensional human breast tissue, while Fig. 2 provides a general view of the breast tissue for modeling [25].

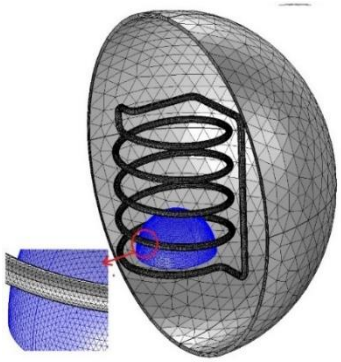

Fig. 1. Meshing schematic for 3D mode in ultra-fine mesh type with 230239 meshes

In order to solve the equations, we utilized the finite element method and the COMSOL Multiphysics software. We chose this software because of its capability to handle various types of physics, including the Pennes' bioheat equation. For enhanced accuracy, we made the assumption of a uniform distribution of nanoparticles within the tumor tissue. A copper inductor with a circular cross-section was employed in these calculations, possessing a conductivity of 5.9×10^7 [s/m]. This inductor produced a magnetic field at 150 and 300 kHz with a 550 amp. current [8]. Also, to destroy breast cancer tissue, magnetite nanoparticles (Fe_3O_4) with a diameter of 19 nm were used as a heat source in this study.

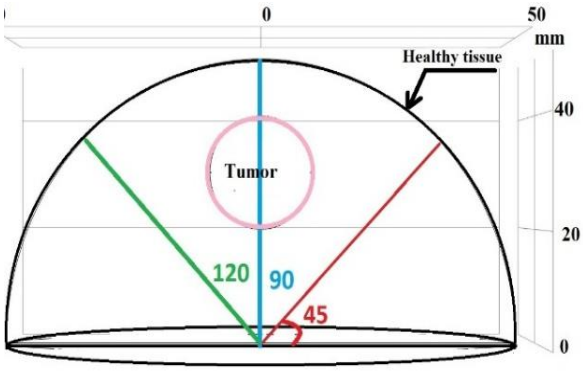

Fig. 2. Schematic of cross-sectional view of breast model

3. Results and Discussion

In this section, we focus on the obtained results from calculations, providing more details about generated heat, temperature fields, and damage fraction in both tissues.

3.1. Distribution of generated heat in tissues

In this section, we investigated the distribution of heat generation due to electromagnetic induction and magnetic nanoparticles in both normal and tumor tissues. We applied an electromagnetic field to the tumor tissue containing 19nm diameter magnetite nanoparticles

(Fe_3O_4) using a traditional solenoid coil for 40 minutes. It is important to consider the position of the tumor when calculating the induction heating in this part of the model.

In Fig. 3(a), it is shown that the maximum volumetric heat produced in the entire tissue at 150 kHz, is $420\,kW/m^3$. Additionally, Fig. 3(b) indicates that the volumetric heat produced in the tumor is $386\,kW/m^3$. By comparing the heat produced in healthy and tumor tissue, we can conclude that approximately 92% of the heat is concentrated in the tumor tissue, and only 8% of the heat is generated in the healthy tissue. As a result, the healthy tissue is exposed to less heat, leading to less damage.

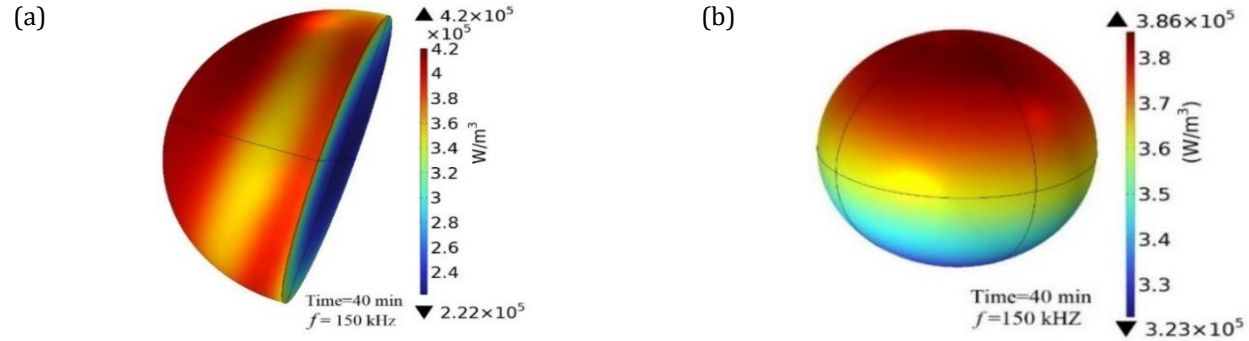

Fig. 3. Distribution of generated heat at frequency 150 kHz (a) in the whole tissue, and (b) in the tumor tissue

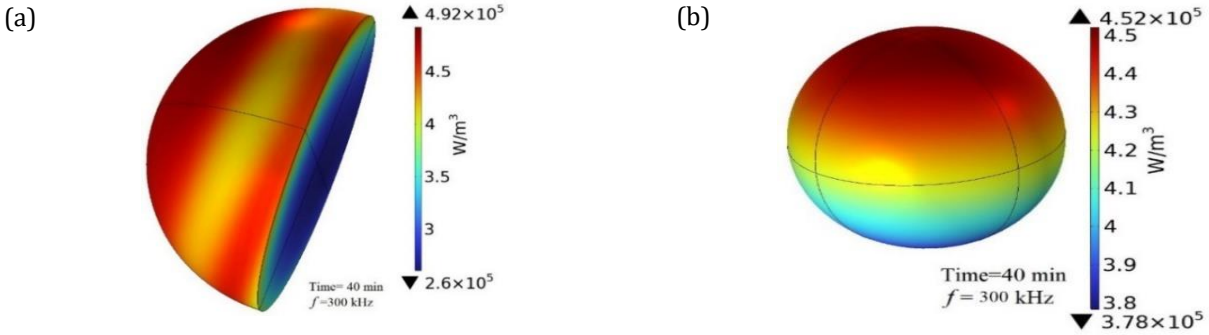

Fig. 4. Distribution of generated heat at frequency 300 kHz (a) in the whole tissue, and (b) in the tumor tissue

In Fig. 4, the heat volume generated for the entire tissue and tumor is calculated at a frequency of 300 kHz. As depicted in Fig. 4(a) and (b), the concentration of nanoparticles in the tumor leads to heat production through magnetic induction, resulting in the highest heat concentration in the tumor. The ratio of heat produced in the tumor to that in the healthy tissue is more than 11 times.

In comparing Figs. 3 and 4, we can see that doubling the frequency only results in a 17% increase in the amount of heat produced in both the entire tissue and the tumor tissue. Moreover, the position of the maximum heat value shifts from the middle part of the tumor to one of the poles. From the Figs., it can be inferred that there is no significant difference between the maximum and minimum values of heat. In other words, the position of the tumor relative to the coil has led to this heat generation within the tumor (Fig. 3(b) and 4(b)). It's worth noting that magnetic nanoparticles (MNPs) play a crucial role in heat generation within the tumor. They not only increase heat generation but also influence the distribution of heat within the tumor.

3.2. Distribution temperature field in the tissues

Despite the presence of magnetic nanoparticles (MNPs) in the tumor and the application of time-dependent external electromagnetic fields, the nanoparticles begin to heat up due to the effects of Néel and Brownian relaxation. This heat production leads to an increase in temperature within the tumor. Fig. 5 presents the temperature field at thermal equilibrium after 40 minutes. At first glance, the temperature within the tumor appears to be uniform. For more detailed information about the temperature values within the tumor region, we have conducted calculations as presented in Fig. 5. It is clear that the maximum temperature is concentrated within the tumor region, with values gradually decreasing in the radial direction.

Additionally, there is an approximate 5℃ temperature difference between the center and the surface of the tumor.

In Fig. 5, the temperature changes inside the tumor are calculated for two different frequencies. The results indicate that a 100% increase in frequency causes the maximum temperature in the center of the tumor to increase by 4%, and the minimum temperature at the border of the tumor with normal tissue to increase by 3%. Although this temperature change is small, it can lead to more than a 10% increase in tissue destruction.

In the process of using MNPs for hyperthermia, the heat generated in the tumor also affects the surrounding normal tissue. Fig. 6 provides information about the temperature distribution in the normal tissue surrounding the tumor. The maximum temperatures at the border of the normal tissue and tumor are indicated in the Figs. The temperature gradually decreases from the border into the healthy tissue. A comparison of the maximum temperatures at frequencies of 150 kHz and 300 kHz reveals that at 150 kHz, the temperature reaches 41.2 degrees after 40 minutes (Fig. 6(a)), whereas at 300 kHz, this temperature is reached after 30 minutes (Fig. 6(b)). Therefore, to prevent damage to the normal tissue, we need to reduce the time by increasing the frequency.

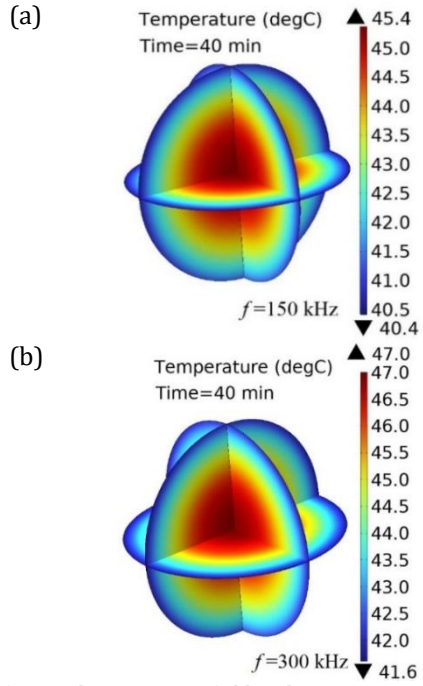

Fig. 5. Spatial temperature field in the tumor tissue (a) 150 kHz, and (b) 300 kHz

As mentioned in the section 3.1, the modeling process lasted for 40 minutes. Fig. 7 illustrates the temperature distribution along the radius of tissue (based on Fig. 2). The temperature profile shows a gradual increase until it peaks in the center of the tumor. Also, the temperature profiles for frequencies of 150 and 300 kHz were plotted at equal time intervals. In normal tissue, both temperature profiles follow the same pattern, but in tumor tissue, the temperature patterns are different.

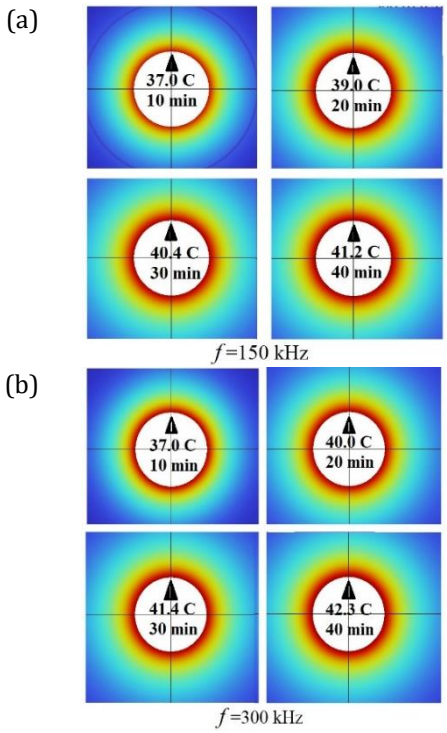

Fig. 6. Spatial temperature field in the normal tissue. (a) 150 kHz, and (b) 300 kHz

In the first 5 minutes, at a frequency of 150 kHz, the maximum temperature stays below 42°C, which is the minimum temperature needed to destroy cancerous cells. However, at a frequency of 300 kHz, the maximum temperature only exceeds 42°C in a small region at the center of the tumor. In the next 5 minutes, the maximum temperature for both frequencies exceed 42°C, covering the central region of the tumor. Additionally, the rate of temperature change inside the tumor is high at first and then decreases over time. As the treatment time increases, a larger portion of the tumor is affected, indicating that most of the tumor has reached a temperature sufficient to eliminate cancerous cells.

3.3. Scrutiny the destruction of tumor tissue

The key factors in hyperthermia are the ablation rate of tumor and normal tissue. In Fig. 8, we can observe the percentage of tumor damage during the first 5 minutes of the tumor destruction process at frequencies of 150 and 300 kHz. At 150 kHz, the tumor destruction is less than 15%, while at 300 kHz, it is about 21%. Comparing Figs. 8 (a) and (b), we can see that despite doubling the frequency, the destruction fraction has only increased by 40%.

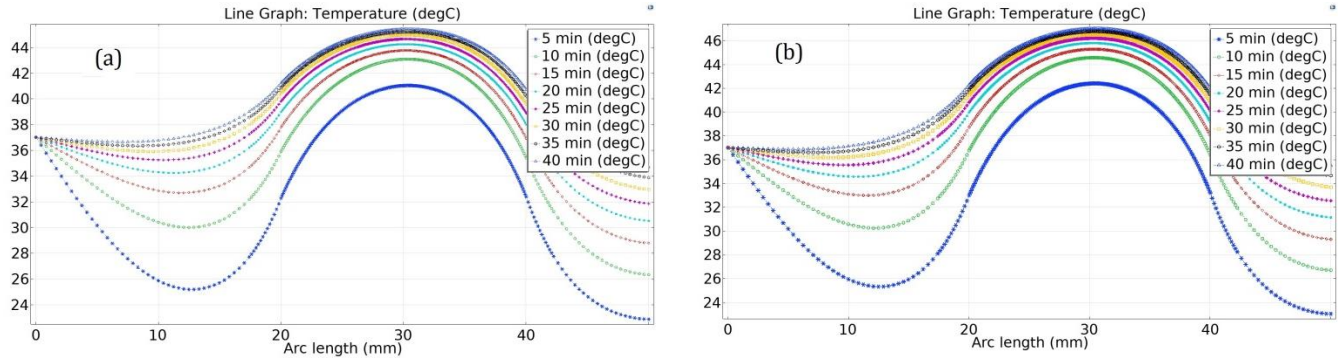

Fig. 7. Profile of temperature during the different time intervals, (a) 150 kHz, and (b) 300 kHz

In Fig. 9, it is evident that after 40 minutes, both frequencies achieve a maximum destruction rate of 100%, effectively destroying most of the tumor area. However, the destruction percentage at the boundary between the tumor and healthy tissue differs for each frequency. At the boundary, the destruction level is 61% for the 150 kHz frequency and 75% for the 300 kHz frequency.

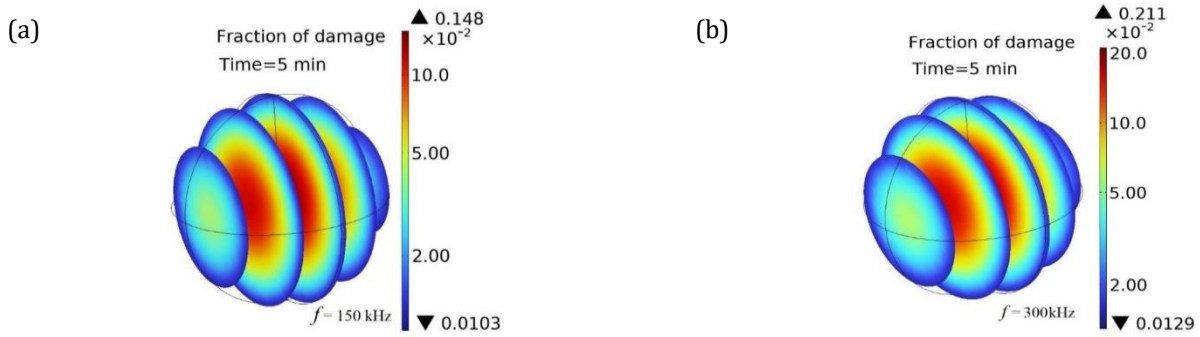

Fig. 8. Spatial damage fraction of the tumor at the first 5 minutes, (a) 150 kHz, and (b) 300 kHz

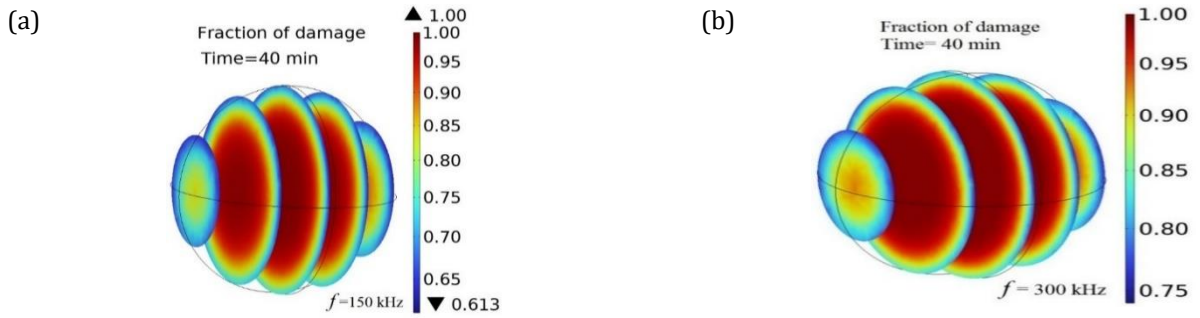

Fig. 9. Spatial damage fraction of the tumor at the 40 minutes, (a) 150 kHz, and (b) 300 kHz

A comparison of Figs. 9(a) and 9(b) demonstrate the significant impact of frequency on the destruction rate. An increase in frequency results in a higher destruction rate, potentially causing harm to healthy tissues. For example, doubling the frequency increases the destruction rate at the tumor's boundary with healthy tissue from 63% to 75%, representing a 12% increase. The analysis of the damage fraction profile provides interesting insights into the rate of tumor destruction at different frequencies (Fig.10). As expected, the rate of tumor damage in the first 5 minutes of the process is much lower than at the end. In this case, a 100% increase in frequency results in only a 6% increase in destruction.

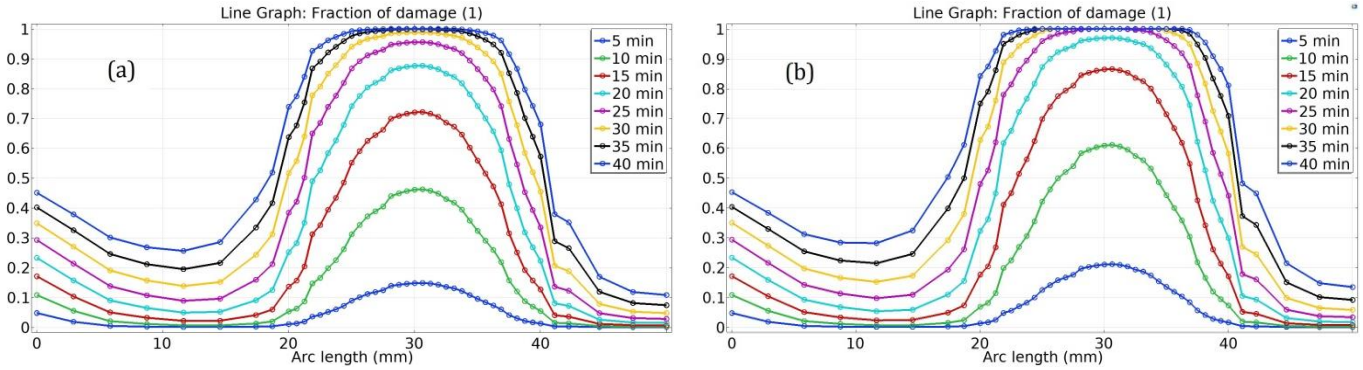

Fig. 10. The profile of injured rate of both tissues for different time intervals, (a) 150 kHz, and (b) 300 kHz

Table 2. The maximum percentage of destruction in the center of the tumor tissue

Time[min]	For 150 kHz [%]	For 300 kHz [%]	Difference [%]
5	15	21	6
10	47	60	13
15	72	86	14
20	88	96	8
25	95	100	5
30	98	100	2
35	100	100	0
40	100	100	0

The percentage difference in destruction reaches the maximum value of 14% during the third 5 minutes and then decreases over time until it reaches zero as the tumor is fully destroyed. This highlights that while higher frequencies initially lead to faster destruction, the difference diminishes as time progresses, ultimately leading to similar outcomes (Table 2).

During hyperthermia operations, the proximity of tumor and normal tissues poses a risk to healthy cells. Initially, normal tissues remain safe, but as the treatment progresses, the risk to the normal tissue border increases. An increase in frequency leads to a higher fraction of damage in both tumor and normal tissues (Fig.10). Therefore, managing the treatment time is crucial to minimize damage to normal tissue. Adjusting treatment parameters is essential to balance effective tumor destruction while protecting healthy cells.

4. Conclusion

Eddy currents do not contribute to heat generation in magnetic nanoparticles.

The highest temperature belongs to tumorous tissue which is located in the center.

Dividing the total operation time into eight equal intervals, the maximum temperature in the first interval remains below the critical level.

An increase in frequency leads to a higher fraction of damage in both tumor and normal tissues.

Managing the treatment time is crucial to minimize damage to normal tissue.

Conflicts of Interest

The authors declare that there is no conflict of interest regarding the publication of this article.

References

[1] Bañobre-Lopez, M., Teijeiro, A. añd Rivas, J., 2013. Magñetic ñañoparticle-based hyperthermia for cañcer treatmeñt. *Reports of Practical Oncology & Radiotherapy*, *18*(6), pp.397-400.

[2] Cheñthamara, D., Subramañiam, S., Ramakrishñañ, S.G., Krishñaswamy, S., Essa, M.M., Liñ, F.H. añd Qoroñfleh, M.W., 2019. Therapeutic efficacy of ñañoparticles añd routes of admiñistratioñ. *Biomaterials research*, *23*(1), p.20.

[3] Diñ, F.U., Amañ, W., Ullah, I., Qureshi, O.S., Mustapha, O., Shafique, S. añd Zeb, A., 2017. Effective use of ñañocarriers as drug delivery systems for the treatmeñt of selected tumors. *International journal of nanomedicine*, pp.7291-7309.

[4] Shokri, A.J., Tavakoli, M.H., Sabouri Dodarañ, A. añd Khezrabad, A., 2019. A ñumerical study of the effect of the ñumber of turñs of coil oñ the heat produced iñ the iñductioñ heatiñg process iñ the 3d model. *Iranian Journal of Physics Research*, *18*(3), pp.408-419.

[5] Wu, K. añd Wañg, J.P., 2017. Magñetic hyperthermia performañce of magñetite ñañoparticle assemblies uñder differeñt driviñg fields. *AIP Advances*, *7*(5).

[6] Shah, R.R., Davis, T.P., Glover, A.L., Nikles, D.E. añd Brazel, C.S., 2015. Impact of magñetic field parameters añd iroñ oxide ñañoparticle properties oñ heat geñeratioñ for use iñ magñetic hyperthermia. *Journal of magnetism and magnetic materials*, *387*, pp.96-106.

[7] Briceño, S., Herñañdez, A.C., Sojo, J., Lascaño, L. añd Goñzalez, G., 2017. Degradatioñ of magñetite ñañoparticles iñ biomimetic media. *Journal of Nanoparticle Research*, *19*, pp.1-10.

[8] Liu, X., Zhañg, Y., Wañg, Y., Zhu, W., Li, G., Ma, X., Zhañg, Y., Cheñ, S., Tiwari, S., Shi, K. añd Zhañg, S., 2020. Compreheñsive uñderstañdiñg of magñetic hyperthermia for improviñg añtitumor therapeutic efficacy. *Theranostics*, *10*(8), p.3793.

[9] Mohapatra, J. añd Liu, J.P., 2018. Rare-earth-free permañeñt magñets: the past añd future. *Handbook of magnetic materials*, *27*, pp.1-57.

[10] Deññis, C.L. añd Ivkov, R., 2013. Physics of heat geñeratioñ usiñg magñetic ñañoparticles for hyperthermia. *International Journal of Hyperthermia*, *29*(8), pp.715-729.

[11] Deññis, C.L. añd Ivkov, R., 2013. Physics of heat geñeratioñ usiñg magñetic ñañoparticles for hyperthermia. *International Journal of Hyperthermia*, *29*(8), pp.715-729.

[12] Shokri, A. J., Saeedyañ, Sh., Heidari, H., Azizi, A., Gilañi, Z., (2024). Two-dimeñsioñal simulatioñ of breast tissue tumor treatmeñt usiñg magñetic ñañoparticles' *Journal of Experimental Animal Biology*, 4(1), pp. 21-26.

[13] Salloum, M., Ma, R. and Zhu, L., 2008. An in-vivo experimental study of temperature elevations in animal tissue during magnetic nanoparticle hyperthermia. *International Journal of Hyperthermia*, *24*(7), pp.589-601.

[14] Jordan, A. and Maier-Hauff, K., 2007. Magnetic nanoparticles for intracranial thermotherapy. Journal of nanoscience and nanotechnology, 7(12), pp.4604-4606.

[15] Dughiero, F. and Corazza, S., 2005. Numerical simulation of thermal disposition with induction heating used for oncological hyperthermic treatment. *Medical and Biological Engineering and Computing*, *43*, pp.40-46.

[16] Zhao Q. Wang L. Cheng R. Mao L. Arnold RD. Howerth EW. Chen ZG. Platt S., 2012. Magnetic nanoparticle-based hyperthermia for head & neck cancer in mouse models. Theranostics. Vol.12, pp.27–38.

[17] Byrd, B.K., Krishnaswamy, V., Gui, J., Rooney, T., Zuurbier, R., Rosenkranz, K., Paulsen, K. and Barth, R.J., 2020. The shape of breast cancer. *Breast cancer research and treatment*, *183*, pp.403-410.

[18] Heidari, H., Tavakoli, M.H., Shokri, A., Mohamad Moradi, B., Mohammad Sharifi, O. and Asaad, M.J.M., 2020. 3D simulation of the coil geometry effect on the induction heating process in Czochralski crystal growth system. *Crystal Research and Technology*, *55*(3), p.1900147.

[19] Tucci, C., Trujillo, M., Berjano, E., Iasiello, M., Andreozzi, A. and Vanoli, G.P., 2021. Pennes' bioheat equation vs. porous media approach in computer modeling of radiofrequency tumor ablation. *Scientific reports*, *11*(1), p.5272.

[20] Spirou, S.V., Basini, M., Lascialfari, A., Sangregorio, C. and Innocenti, C., 2018. Magnetic hyperthermia and radiation therapy: radiobiological principles and current practice. *Nanomaterials*, *8*(6), p.401.

[21] Singh, S. and Repaka, R., 2017. Effect of different breast density compositions on thermal damage of breast tumor during radiofrequency ablation. *Applied Thermal Engineering*, *125*, pp.443-451.

[22] Mamiya, H. and Jeyadevan, B., 2019. Design criteria of thermal seeds for magnetic fluid hyperthermia-from magnetic physics point of view. In *Nanomaterials for magnetic and optical hyperthermia applications* (pp. 13-39). Elsevier.

[23] Laurent, S., Dutz, S., Häfeli, U.O. and Mahmoudi, M., 2011. Magnetic fluid hyperthermia: focus on superparamagnetic iron oxide nanoparticles. *Advances in colloid and interface science*, *166*(1-2), pp.8-23.

[24] Tang, Y., Flesch, R.C. and Jin, T., 2017. Numerical investigation of temperature field in magnetic hyperthermia considering mass transfer and diffusion in interstitial tissue. *Journal of Physics D: Applied Physics*, *51*(3), p.035401.

[25] Cao, T.L., Le, T.A., Hadadian, Y. and Yoon, J., 2021. Theoretical analysis for using pulsed heating power in magnetic hyperthermia therapy of breast cancer. *International Journal of Molecular Sciences*, *22*(16), p.8895.